Monthly Notices
of the
ROYAL ASTRONOMICAL SOCIETY

MNRAS **476,** 4501–4509 (2018) doi:10.1093/mnras/sty534
Advance Access publication 2018 February 27

The hELENa project – II. Abundance distribution trends of early-type galaxies: from dwarfs to giants

A. Sybilska,[1,2]★ H. Kuntschner,[2] G. van de Ven,[3] A. Vazdekis,[4,5] J. Falcón-Barroso,[4,5] R. F. Peletier[6] and T. Lisker[7]

[1]*Baltic Institute of Technology, al. Zwycistwa 96/98, PL-81-451 Gdynia, Poland*
[2]*European Southern Observatory, Karl-Schwarzschild-Strasse 2, D-85748 Garching bei München, Germany*
[3]*Max Planck Institute for Astronomy, Königstuhl 17, D-69117 Heidelberg, Germany*
[4]*Instituto de Astrofísica de Canarias, Vía Láctea s/n, E-38205 La Laguna, Tenerife, Spain*
[5]*Departamento de Astrofísica, Universidad de La Laguna, E-38200 La Laguna, Tenerife, Spain*
[6]*Kapteyn Astronomical Institute, University of Groningen, Postbus 800, NL-9700 AV Groningen, the Netherlands*
[7]*Astronomisches Rechen-Institut, Zentrum für Astronomie der Universität Heidelberg, Mönchhofstrasse 12-14, D-69120 Heidelberg, Germany*

Accepted 2018 February 15. Received 2018 February 1; in original form 2017 August 2

ABSTRACT

In this second paper of T*h*e role of *E*nvironment in shaping *L*ow-mass *E*arly-type *N*earby g*a*laxies (hELENa) series we study [Mg/Fe] abundance distribution trends of early-type galaxies (ETGs) observed with the Spectrographic Areal Unit for Research on Optical Nebulae integral field unit, spanning a wide range in mass and local environment densities: 20 low-mass early types (dEs) of Sybilska et al. and 258 massive early types (ETGs) of the ATLAS^{3D} project, all homogeneously reduced and analysed. We show that the [Mg/Fe] ratios scale with velocity dispersion (σ) at fixed [Fe/H] and that they evolve with [Fe/H] along similar paths for all early types, grouped in bins of increasing local and global σ, as well as the second velocity moment $V_{\rm rms}$, indicating a common inside-out formation pattern. We then place our dEs on the [Mg/Fe] versus [Fe/H] diagram of Local Group galaxies and show that dEs occupy the same region and show a similar trend line slope in the diagram as the high-metallicity stars of the Milky Way and the Large Magellanic Cloud. This finding extends the similar trend found for dwarf spheroidal versus dwarf irregular galaxies and supports the notion that dEs have evolved from late-type galaxies that have lost their gas at a point of their evolution, which likely coincided with them entering denser environments.

Key words: galaxies: abundances – galaxies: dwarf – galaxies: evolution – galaxies: stellar content – galaxies: structure.

1 INTRODUCTION

Detailed studies of galaxy properties as a function of redshift are hampered by the low signal-to-noise ratio (SNR) and low spatial resolution of high-redshift data. In order to study galaxy evolution we thus often turn to nearby galaxies to perform detailed studies of their stellar populations, with the hope to unveiling their evolutionary details through their star formation histories (SFHs). This so-called 'stellar archaeology' method has traditionally been limited by the age–metallicity degeneracy when deriving population properties from broad-band colours. Using absorption line indices makes it possible, in principle, to lift the degeneracy, though here the challenge lies in ensuring that the derived metallicities are not affected by inherent abundance ratios. This, in turn, can be tackled by using abundance-ratio-independent index combinations (e.g. Kuntschner et al. 2010) and stellar population models specifically allowing for varying abundance ratios (e.g. Thomas et al. 2005).

The relation between element abundance ratios and metallicity has been studied in detail (through resolved observations) mostly for dwarf spheroidal galaxies (dSphs) of the Milky Way (MW) due to their proximity to our Galaxy (see e.g. Kirby et al. 2011b or the review of Tolstoy, Hill & Tosi 2009). Some data also exist for Local Group (LG) dwarf irregular galaxies (dIrrs), however, owing to their larger line-of-sight distances we are not able to study individual stars as faint as in the case of the closer dSphs, meaning the available samples do not cover comparably low-metallicity regimes.

Beyond the LG the situation is yet more complicated. Unable to obtain spectroscopic data for individual stars we need to resort to integrated measurements of stellar population parameters. These do not allow for the same level of detail to be examined since at each

★ E-mail: sybilska.aga@gmail.com

Table 1. Basic details of the literature samples used in the study.

Data type	Source	Sample info	Instrument	Mass range ($M_\odot$)
Unresolved/IFU	Sybilska et al. (2017)	20 dEs, Virgo and field	SAURON/WHT	1.68×10^9–8.18×10^9 [a]
	Scott et al. (2013)	258 ETGs, Virgo and field	SAURON/WHT	3.86×10^9–5.96×10^{11} [b]
Resolved	Tolstoy et al. (2009)[g]	Sculptor	UVES/VLT	$1.3 \pm 0.3, 2.3 \pm 0.2 \times 10^7$ [c]
		Fornax	UVES/VLT, FLAMES/VLT	$5.3 \pm 0.6, 7.4 \pm 0.4 \times 10^7$ [c]
		Carina	UVES/VLT	$0.6 \pm 0.2, 1.0 \pm 0.1 \times 10^7$ [c]
		Sagittarius	HIRES/Keck, FLAMES/VLT, UVES/VLT	1×10^9 [d]
	Kirby et al. (2011a)	Sculptor	DEIMOS/Keck	$1.3 \pm 0.3, 2.3 \pm 0.2 \times 10^7$ [c]
		Leo I	DEIMOS/Keck	$1.2 \pm 0.3, 2.2 \pm 0.2 \times 10^7$ [c]
	Pompéia et al. (2008)	LMC	FLAMES/VLT	$1.7 \pm 0.7 \times 10^{10}$ [e]
	Bensby et al. (2014)	Milky Way	FEROS/ESO 1.5 m, 2.2 m; SOFIN, FIES/NOT; UVES/VLT; HARPS/ESO 3.6 m; MIKE/Magellan Clay Telescope	$1.39 \pm 0.49 \times 10^{12}$ [f]

Notes. [a] $M_{\rm vir}$ mass range based on $R_{\rm e}$ and σ values of Sybilska et al. (2017).
[b] $M_{\rm JAM}$ mass range from Cappellari et al. (2013).
[c] $M_{1/2}$ from Collins et al. (2014) and Wolf et al. (2010), respectively.
[d] Total mass of the best-fitting cuspy/core model from Majewski et al. (2013).
[e] M (8.7 kpc) from van der Marel & Kallivayalil (2014).
[f] M_{100} mass of Watkins, Evans & An (2010).
[g] Compiled from Shetrone et al. (2003), Geisler et al. (2005), McWilliam & Smecker-Hane (2005), Letarte (2007), Sbordone et al. (2007), and Koch et al. (2008).

spatial point we get integrated, light-weighted information on all the underlying populations at that location. Nevertheless, with the help of stellar population models and various SFH recovery techniques we may still get insight into the assembly of those galaxies across the cosmic time.

[Mg/Fe] abundance ratio is one of the fundamental measures of chemical enrichment in galaxies since different elements are produced in processes of different time-scales, in this case Type Ia versus Type II supernovae (SNe), each having progenitors of different masses. Thus, the relation between [Mg/Fe] and [Fe/H] can provide information on the amount of feedback from the various SNe types and is expected to be constant for the lowest metallicity values, i.e. before Type Ia SNe start contributing to the chemical evolution producing α elements. The downward turn of the [Mg/Fe] versus [Fe/H] trend seen in the resolved MW data is known as a 'knee' and is an indication of the metal enrichment achieved up to that point in time (i.e. how efficient star formation was during the first $\sim$1 Gyr of the galaxy evolution), thus, for example, a lower [Fe/H] at the knee location means lower feedback from star formation. This could be due to more mass being locked up in low-mass stars or e.g. galactic winds causing outflow of metal-enhanced material (e.g. Tolstoy et al. 2009).

The knee location can only be determined for galaxies for which very metal-poor stars can be spectroscopically observed, which has so far only been achieved for the MW. Such metal-poor stars are still mostly out of reach for extragalactic objects, even those in the LG. Their large line-of-sight distances mean only the brightest stars can be observed, which dramatically limits the lookback time. Much outside of the LG we do not even have the luxury of individual star spectroscopic measurements and need to rely on integrated spectra. Theoretically, we would be able to obtain very low metallicity measurements only if the entire probed galaxy region was composed of the oldest, metal-poorest stars.[1]

[1] We note, however, that with the use of techniques such as full-spectrum fitting (e.g. Koleva et al. 2009) one could, in principle, be able to detect an old, metal-poor underlying population if it were sufficiently massive.

Nevertheless, we can still benefit from the analysis of the [Mg/Fe] versus [Fe/H] profiles and trends of various galaxy types across large mass ranges and different environments. Differences in the observed abundances contain clues as to the efficiency of internal enrichment mechanisms or the influence of environmental factors such as accretion or mergers. For example, a low [α/Fe] at low [Fe/H] could indicate accretion of stellar material from objects where star formation efficiency was lower (e.g. Wyse 2010). The analysis of the loci of points and locations of the [Mg/Fe] versus [Fe/H] profiles (at the high-metallicity end) can thus provide insight into differences between SFHs of the studied objects.

2 SAMPLE SELECTION

Below we provide a description of the literature samples used in the present study, which includes integral field unit (IFU) spectroscopic data for a total of 278 galaxies in the Virgo Cluster and the group/field environment, as well as resolved data for MW and a number of LG galaxies. Individual references are provided below and in Table 1.

2.1 Integrated-light data

All our IFU data have been obtained with the Spectrographic Areal Unit for Research on Optical Nebulae (SAURON) IFU at the William Herschel Telescope (WHT) in La Palma, Spain. The data reach out to ca. 1 effective radius ($R_{\rm e}$) and their spatial extent is limited either by field of view (FoV) of the SAURON instrument [for most of the ATLAS$^{\rm 3D}$ sample and some dwarf elliptical galaxies (dEs)] or the per-spaxel SNR (for dEs set to 7 and roughly corresponding to surface brightness of $\mu_V \approx 23.5$ mag at the edge of the field). For details on the sample selection and data reduction see the relevant papers cited below. Below we provide a short summary for the reader's convenience.

Our low-mass early-type sample consists of 20 dwarf early types (dEs; Sybilska et al. 2017, hereafter S17), 17 of which are located in the Virgo Cluster and three in the field. The galaxies have been drawn from the high-mass end of the dE luminosity function and

comprise objects of various dE subtypes (discy, blue core, as well as nucleated and non-nucleated galaxies), as well as a range of ellipticities and locations within the Virgo Cluster.

The massive early-type sample consists of 258 ATLAS^{3D} galaxies: 58 Virgo Cluster and 200 field/group objects. The population parameters presented here are, as described in S17, based on the line strength measurements of Scott et al. (2013), which were transformed from the Lick to the Line Index System (LIS) system of Vazdekis et al. (2010) and for which stellar population estimates were then derived using MILES stellar population models (Vazdekis et al. 2015) in order to ensure maximal homogeneity. We also compare these population measurements to those for the same sample but derived with the use of Schiavon (2007) models (Kuntschner et al., in preparation) to check for consistency – see the appendix of S17 for details.

2.2 Resolved data

Data for LG dSphs were taken from the works of Tolstoy et al. (2009) and Kirby et al. (2011b). For these data sets we either directly took the provided moving averages/average profiles or calculated them ourselves. Additionally, we include the data from Pompéia et al. (2008) on the Large Magellanic Cloud (LMC) and from Bensby, Feltzing & Oey (2014) for the MW. We average the values of the latter so that an average trend line similar to those for early types could be shown. The moving averages for the MW and the IFU sample were created by using a fixed subset with the size dependent on the number of available points.

3 METHODS

3.1 Deriving radial profiles

Similar to stellar population profiles of S17, radial profiles of σ, $V_{\rm rms} = \sqrt{V^2 + \sigma^2}$ were obtained from the S17 kinematic maps by averaging bins[2] in elliptical annuli (i.e. along the lines of constant surface brightness) of increasing width, equal in log space. The same method was used by Kuntschner et al. (2006, 2010) for the SAURON survey and subsequently by Scott et al. (2013) for the ATLAS^{3D} sample, with which we compare our results here. The errors on the averaged quantities were then obtained by taking a standard deviation of the values corresponding to the individual bins included in a given annulus. Population parameters were then derived from these annuli-averaged values.

3.2 Determining stellar population parameters of the IFU samples

The methods for the derivation of [M/H] and [Mg/Fe] abundance ratios are described in sections 3.6 and 3.7 of S17. In short, we use the abundance ratio insensitive index combination [MgFe50]' of Kuntschner et al. (2010) and the optimized H $\beta_{\rm o}$ index defined by Cervantes & Vazdekis (2009), which is less dependent on metallicity than the traditional Hβ index. We then derive age and metallicity ([M/H]) with the help of MILES stellar population models of Vazdekis et al. (2015), linearly interpolating between the available model prediction. To reduce the effects of grid discretization, we oversample the original models using a linear interpolation in the age–[M/H]-[index] space. [Fe/H] values are subsequently calculated using the following formula: [Fe/H] = [M/H] − 0.75 × [Mg/Fe] (ibid.).

To derive the [Mg/Fe] abundance ratios we interpolate between the predictions of MILES scaled-solar and α-enhanced models on the Mg b–Fe5015 plane. For each line strength measurement we extract Mg b and Fe5015 index pairs from both sets of models, corresponding to the best-fitting single stellar population (SSP) age and metallicity derived by interpolating between model predictions in the H$\beta_{\rm o}$–[MgFe50] plane. We then calculate the distance between the two points and the distance between the points and our measured value to obtain the estimate of the [Mg/Fe] enhancement.

While in principle the Fe5270 is more commonly chosen for the derivation of population parameters, the SAURON wavelength range is such that the index can only be measured for a small subsample of our galaxies (depending on their redshift). Kuntschner et al. (2010, their fig. 4) have, however, shown for central apertures of their galaxies that the abundance ratios derived with the help of the two metal lines give consistent results.

We do note that the choice of models can influence the derived stellar population parameters values and introduce systematic bias. For example, a grid that is less orthogonal (i.e. shows a larger age–metallicity correlation) is able to systematically bias the derived parameters towards older ages or lower metallicities, and as a result influence the shape of the derived population profiles, an example of which can be seen in fig. 3 of Kuntschner et al. (2010). On the other hand, as shown in fig. 6 of the same paper, metallicity and abundance ratio do not suffer from a degeneracy (error correlation) when analysed together, hence the choice of these two stellar population parameters is justified and the [Mg/Fe] versus [Fe/H] plane is a robust one to work with. This is further substantiated for the relative comparison of all our IFU data, given the same instrument and analysis approach for the entire sample.

For a comparison between the stellar population values obtained for the ATLAS^{3D} sample using the Lick system and Schiavon (2007) models versus the values presented here, see the appendix of S17.

3.3 Comparing resolved and unresolved observations

3.3.1 Globular cluster studies

A number of recent studies have investigated the issue of comparability of metallicity and abundance ratio values obtained using integrated-light (IL) spectroscopic measurements versus high-resolution spectroscopy of individual stars in Galactic or LG globular clusters (GCs).

Based on a sample of 23 Galactic GCs Pipino & Danziger (2011) provide empirical calibrations for a conversion of Lick indices into abundances for the IL of old SSPs for a large range of observed [Fe/H] and [α/H]. Their discussion on problems with the derivation of true [Mg/Fe] ratio applies only to the very low (<-1) [Fe/H] regime, not applicable in our case (except for one galaxy). The expected underestimation of [Mg/Fe] is 0.05 dex, which is within our measurement errors.

Sakari & Wallerstein (2016) analyse 25 M31 GCs comparing results from their H-band IL spectral measurements and high-resolution optical values from Colucci, Bernstein & Cohen (2014). The relation showing the difference in the [Mg/Fe] values obtained using the two data sets as a function of [Fe/H] is shown in their fig. 8 and has a mean offset of −0.02 and a standard deviation of 0.16. Additionally, a comparison of their H-band results to low-resolution Lick index values from Schiavon et al. (2013) shows a

[2] The maps were Voronoi binned to a minimum of S/N = 30; see S17 for more details.

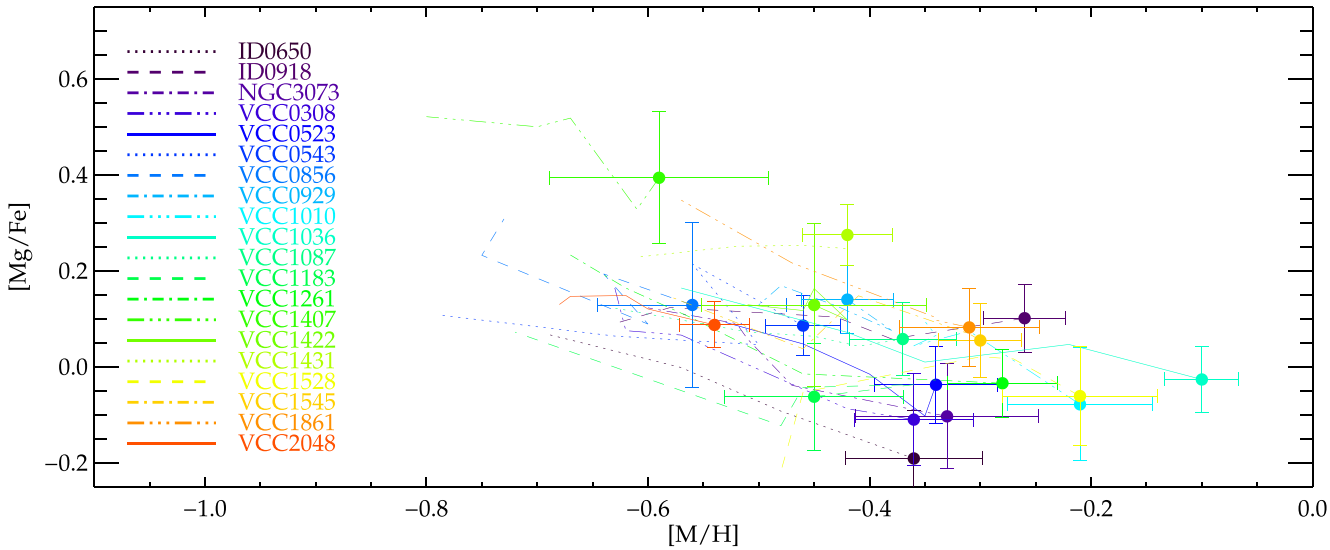

Figure 1. [Mg/Fe] abundance ratio as a function of [M/H] of the 20 low-mass early-type galaxies of S17 from the Virgo Cluster and the field/group environment. The galaxy centres have been marked with filled circles, error bars are shown for central points (the outermost profile points have error bars typically ∼twice as large as the central ones – for the full profiles with uncertainties see the appendix of the above paper).

similarly good agreement between the two (mean offset: 0.0; standard deviation: 0.12).

We note that Colucci, Bernstein & McWilliam (2017) find systematically lower (-0.24 ± 0.07 dex) [Mg/Fe] values from IL than from individual star measurements. However, the offset is less severe (ca. −0.15) for higher (>−1.0) [Fe/H] values. As a possible explanation of the discrepancy they give large abundance differences that might exist in a small fraction of luminous cool giants that dominate IL measurements but perhaps are not represented in the individual stars comparison sample.

The [Fe/H] values measured by Larsen, Brodie & Strader (2017) agree well with the literature values for individual stars from literature compilation (see their table 4 for sources). For [Mg/Fe] they find that their IL values are systematically lower than those of Carretta et al. (2009), the average difference is ca. −0.15 dex, but again, the largest (>0.2 dex) discrepancies are for the very low (<−2) values of [Fe/H], with the average offset for more metal-rich GCs being on average 0.1 dex. A comparison with other sources (Pritzl, Venn & Irwin 2005; Roediger et al. 2014) shows the two types of measurements to agree to within the errors. Additionally, the authors point out that even high-resolution spectroscopy of individual stars have systematic uncertainties of the order of ca. 0.1 dex associated with them, hence an agreement of IL versus individual stars measurements within this tolerance should be considered satisfactory.

3.3.2 Galaxy studies

More generally, the question of the feasibility of IL versus individual star measurements comparison has also been discussed in the context of dwarf and more massive galaxy studies. Makarova et al. (2010) compare resolved *Hubble Space Telescope* (*HST*)/Advanced Camera for Surveys (ACS) and IL data from the 6-m telescope of the Special Astrophysical Observatory of Russian Academy of Sciences for dSps/dEs in the M81 group and find that the two methods (colour–magnitude diagram versus full-spectrum fitting) give consistent [Fe/H] results for both galaxies ([Fe/H] ≈ −1.5), albeit with some discrepancy for the younger, more metal-rich component in one of the objects.

In terms of much younger objects, García-Benito & Pérez-Montero (2012) compare SFHs for a nearby blue compact dwarf galaxy NGC 6789 obtained through the analysis of *HST*/Wide Field and Planetary Camera 2 (WFPC2) photometric and WHT/Intermediate dispersion Spectrograph and Imaging System (ISIS) spectroscopic data and find that they agree to within the errors.

More recently, Ruiz-Lara et al. (2015) carried out a similar test but expanded to systems with more complex SFHs. For a region in the LMC, they compare SFHs based on long-slit data from ESO 3.6 m/EFOSC2 with SFHs based on photometry from *HST*/WFPC2. They conclude that a full-spectrum analysis of IL data is a reliable way of recovering SFHs even in SFH-wise complex systems, providing that a proper set of spectral templates is used.

4 RESULTS

4.1 Virgo and field early-type galaxies

Fig. 1 shows the [Mg/Fe] abundance ratio as a function of [M/H] for each our dE galaxy individually. Looking at these profiles we see that the [Mg/Fe] ratios evolve with metallicity along nearly the same paths for all our dEs (see Kirby et al. 2011b for a similar result for LG dSphs). The values of [Mg/Fe] tend to increase outwards, though the associated gradients are mostly shallow or null to within the errors. [Fe/H] gradients, on the other hand, are all negative, with the majority *not* negligible to within the errors. This has already been shown and quantified in S17 (Paper I of this series) and agrees with the literature (e.g. Koleva et al. 2009 who analysed long-slit data for 16 dEs, belonging to the Fornax Cluster or nearby groups and find strong metallicity gradients for the majority of their sample, as well as Mentz et al. 2016 who show Multi Unit Spectroscopic Explorer (MUSE) IFU data for one Virgo dE and find a gradient in both [Fe/H] and [Mg/Fe]).

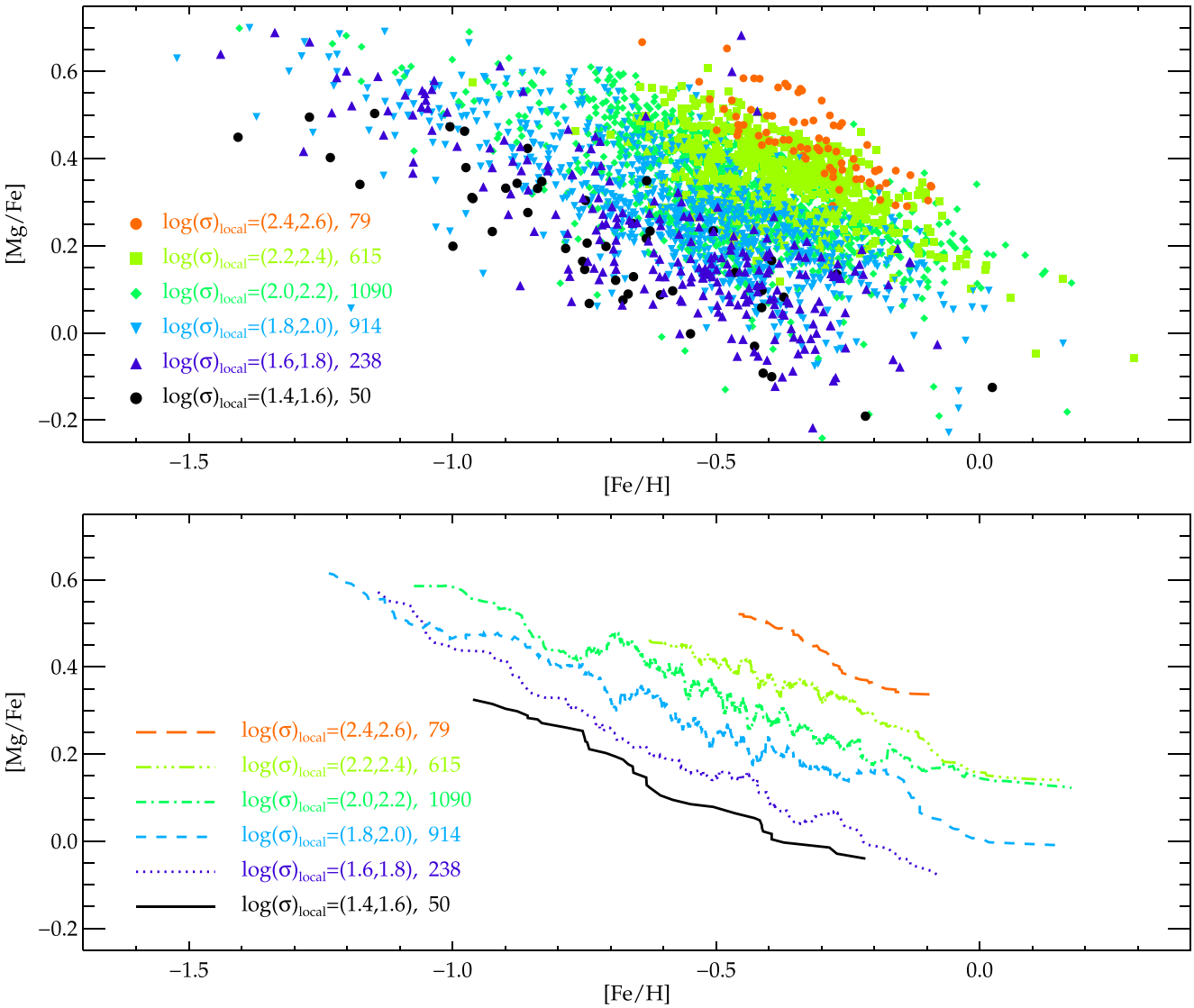

Figure 2. Upper panel: [Mg/Fe] abundance ratio as a function of [Fe/H] for all the profile points from the S17 sample and ATLAS^{3D} galaxies, colour coded by $\sigma_{\rm local}$ values as explained in the legend, with the number of points falling into each bin provided next to the bin ranges. Lower panel: running averages of all the profile points for the above defined σ bins (same colour coding). [Fe/H] values have been obtained from [M/H] using the formula of Vazdekis et al. (2015): [Fe/H] = [M/H] − 0.75 × [Mg/Fe]. Note that the running averages are *not* averaged profiles as they combine points based on their [Fe/H] value and not location in a galaxy: for example, individual galaxies with flat [Mg/Fe] profiles are still able to produce a non-flat running average if their [Mg/Fe] and [Fe/H] values differ among the said galaxies; also, points belonging to one galaxy may be included in running averages for *different* σ bins.

Fig. 2 shows the [Mg/Fe] versus [Fe/H] relation for all individual profile points (upper panel) and running averages (lower panel) for all early-type galaxies (ETGs) in our sample, grouped by local velocity dispersion $\sigma_{\rm local}$. Note that, as also explained in the figure caption, these trend lines show averages for given [Fe/H] values, irrespective of the galaxy regions these correspond to (hence are *not* profiles in the traditional sense), though as we move towards higher σ, the same [Fe/H] *do* typically correspond to regions further away from galaxy centres.

We see that the shape of these [Fe/H]-averaged trend lines is qualitatively similar for all early types, indicating comparable (inside-out) internal evolution. This has been shown earlier for the [Fe/H]–σ and [Mg/Fe]–σ relations separately for these samples (McDermid et al. 2015; S17). However, even compared at fixed metallicity values, the [Mg/Fe] abundance ratios scale with velocity dispersion. Here we also show that the massive galaxies' outskirts, while comparable in metallicity to the centres of dEs, are significantly more Mg enhanced. On the other hand, similar levels of [Mg/Fe] are observed in e.g. outskirts of low-σ as in central parts of high-σ galaxies, with the metallicities of the former significantly below those of the latter.

4.2 Virgo and field ETGs versus Local Group late- and early-types

Our findings expand on those of Mentz et al. (2016) who showed MUSE IFU data for one Virgo dE juxtaposed on literature data for the LG galaxies. Thanks to the much larger wavelength range available in MUSE, the authors were able to study not only Mg but also Na and Ca abundance ratios. In the present work, while limited

to magnesium, we are able to show [Mg/Fe] versus [Fe/H] profiles for a much larger sample of both low- and high-mass early types.

Fig. 3 shows the comparison between the dE galaxies of the previous subsection with the LG dwarfs and the MW. We have transformed the individual literature data points to the shown trends by calculating their running averages as described in Section 2.

We see that LG dEs/dSphs do not reach the [Fe/H] levels of more massive cluster dEs, which is expected from the mass–metallicity relation [see e.g. Tremonti et al. 2004 or Gallazzi et al. 2005 for relations derived from Sloan Digital Sky Survey (SDSS) data for gas phase and stellar metallicities, respectively – which relations, however, do not reach the dSph low-mass levels; as well as Hidalgo 2017 for a M_*–$[\mathrm{Fe/H}]_{\mathrm{RGB}}$ relation for LG dwarfs covering the 10^3–$10^{8.5}$ M_* mass range].

To a first degree of approximation LG dSphs, do, however, show similar levels of [Mg/Fe] enhancement as more massive cluster dEs of the SAURON sample. We also see that the shape of the [Mg/Fe] versus [Fe/H] trend lines is similar for cluster dEs and LG dSphs that are up to two orders of magnitude less massive. This complements the findings of Kirby et al. (2011b) who found that MW dSph satellites' abundance ratios follow roughly the same path with increasing [Fe/H]. We note that our data do not reach as high [Mg/Fe] values as those of LG dSphs. This can possibly stem from the SNR limitations of the IFU data set: if we were to probe regions much beyond $1\,R_{\mathrm{e}}$ (for which most of the IL would likely come from oldest, i.e. high-[Mg/Fe] and low-[Fe/H] stars), it is possible that we would be seeing values of [Mg/Fe] as high as the above also for dEs.

Our dEs occupy roughly the same region of the [Mg/Fe] versus [Fe/H] diagram as the LMC stars and the high-metallicity regions of the MW. A similar finding but for dSPh versus dIrrs was shown in Tolstoy et al. (2009) for (see their fig. 17) which they interpreted as dSphs being consistent with dIrrs that lost their gas at a late stage of their evolution.

5 DISCUSSION AND SUMMARY

We have shown that the chemical enrichment histories of our galaxies resemble those of the MW disc[3] and the LG late-type dwarf LMC in that they occupy the same region in the [Mg/Fe] versus [Fe/H] diagram and the slopes of their [Mg/Fe] versus [Fe/H] trend lines are similar. Following up on the Tolstoy et al. (2009) finding for dSphs and dIrrs discussed earlier, we could argue that dEs extend the trend for late-type galaxies of comparable or higher masses and thus support the notion that dEs have evolved from late-type galaxies that have lost their star-forming material at a point in their evolutionary history, which likely coincided with entering regions of higher environmental density (either groups or clusters). However, with the current data we are unable to put a time stamp on such an event happening.

Low-mass ETGs are known to have lower [Mg/Fe] ratios than massive ETGs (Michielsen et al. 2008; S17) but an even stronger relation exists between mass/σ and metallicity. Thanks to our spatially resolved data, i.e. the availability of local [Fe/H] and [Mg/Fe] values, we are able to show that the relation between σ and [Mg/Fe] holds even at fixed [Fe/H]. Lower [Mg/Fe] at a given [Fe/H] in the case of dEs and LMC indicates an overall less efficient enrichment mechanism(s) as compared with e.g. massive ETGs, since such galaxies have not managed to produce large amounts of metal relative to the available star-building material. This means lower mass galaxies (exhibiting low [Mg/Fe] ratios) are either inefficient at turning gas into stars or they do produce metals but are unable to retain them (and so the new generations of stars are not enriched), either due to galactic winds, or environmental factors such as tidal forces or starvation that are able to stop the star forming process.

For galaxies of similar masses, differences in [Mg/Fe] ratios at fixed [Fe/H] can provide clues on the galaxies' merger histories. Zolotov et al. (2010) find in their simulations that accreted stars, coming from lower mass objects, have lower [O/Fe] values (used as proxy for [α/Fe]) at the high-[Fe/H] end than those stars that were formed in situ. The authors show that differences in [O/Fe] at similar [Fe/H] result from the different potential wells within which in situ and accreted halo stars formed. While the various [α/Fe] versus [Fe/H] relations might differ quantitatively, they all show the same (qualitative) behaviour in that the shape of the above relation shows a downturn at high [Fe/H] ratios (e.g. Tolstoy et al. 2009; Mentz et al. 2016). Therefore, for galaxies of equal masses to have similar [α/Fe] ratios at fixed [Fe/H] would mean that they likely have had similar merger histories – their stars having formed in similarly deep potential wells (unless the processes that affected the ratios managed to cancel each other out): alternatively, a galaxy from the above hypothetical pair but with lower [Mg/Fe], i.e. with a larger portion of its mass contained in stars of lower [Mg/Fe] must have obtained them from smaller mass galaxies through a (series of) minor merger(s). We do not find a significant difference between dEs and LMC, suggesting that – in terms of merger histories – their evolutionary paths could have been similar.

The results presented here are in agreement with those of Mentz et al. (2016) for one dE observed with MUSE, as well as those in Şen et al. (2018) who show central [Mg/Fe] values for 11 Virgo dEs drawn from the SMAKCED project sample (Toloba et al. 2014). Besides [Mg/Fe], these works have been able to examine [Ca/Fe] and [Na/Fe] abundance ratios and noted the difference of the former between their dEs and the LMC. However, a detailed discussion of discrepancies seen in different elements' abundance distributions is beyond the scope of this paper.

Our approach presented here is limited by the SAURON wavelength range to the Fe5015 and Mg b metallicity-tracing indices. To strengthen and expand on our findings, as well as those quoted above, it would therefore be advisable to obtain for our sample spectroscopic data covering a larger wavelength range (such as that available with MUSE) so that other α elements can be studied simultaneously alongside magnesium.

ACKNOWLEDGEMENTS

We thank the anonymous referee whose suggestions and comments helped improve the presentation of the paper results. AS acknowledges the support of the Alexander von Humboldt Foundation through a Humboldt Research Fellowship for post-doctoral researchers and through a Humboldt Return Fellowship. The paper is based on observations obtained at the William Herschel Telescope, operated by the Isaac Newton Group in the Spanish Observatorio del Roque de los Muchachos of the Instituto de Astrofísica de Canarias. We thank Nicholas Scott for making his local velocity dispersion measurements for the ATLAS^{3D} sample available to us. AV and JF-B acknowledge support from grant

[3] We note here that the thin and thick discs of the MW show different trends in [Fe/H]–[α/Fe] diagrams (with [α/Fe] being more enhanced in the latter), though the trend seems less pronounced in the [Mg/Fe]–[Fe/H] relation itself (see e.g. Bensby et al. 2014, section 6, fig. 15 and Bland-Hawthorn & Gerhard 2016, section 5.2.2, and references therein).

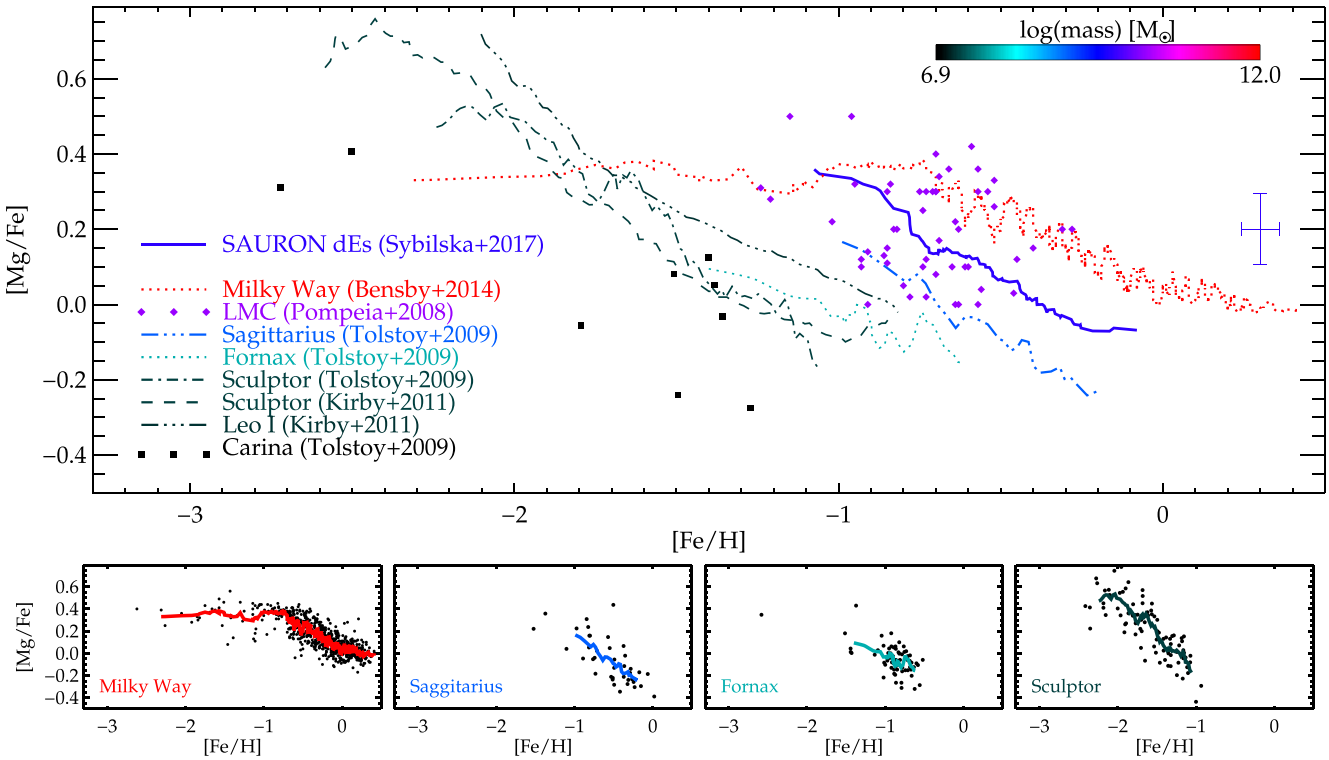

Figure 3. Upper panel:[Mg/Fe] abundance ratio as a function of [Fe/H] for the compilation of literature data on the Milky Way and LG dwarf galaxies, compared with our own data on low-mass early-type galaxies. The galaxies are colour coded according to their dynamical mass as shown in the legend (see Section 2 for details on the mass estimate sources and definitions). Blue cross shown on the right indicates an average error for the dE sample; for errors on individual galaxies see Fig. 1. Lower panel: individual measurements from Tolstoy et al. (2009) and Bensby et al. (2014), overplotted with tracks shown in the upper panel.

AYA2016-77237-C3-1-P from the Spanish Ministry of Economy and Competitiveness (MINECO). RFP and TL acknowledge financial support from the European Union's Horizon 2020 research and innovation programme under the Marie Skłodowska–Curie grant agreement no. 721463 to the SUNDIAL ITN network.

REFERENCES

Bensby T., Feltzing S., Oey M. S., 2014, A&A, 562, A71
Bland-Hawthorn J., Gerhard O., 2016, ARA&A, 54, 529
Cappellari M. et al., 2013, MNRAS, 432, 1709
Carretta E., Bragaglia A., Gratton R., Lucatello S., 2009, A&A, 505, 139
Cervantes J. L., Vazdekis A., 2009, MNRAS, 392, 691
Collins M. L. M. et al., 2014, ApJ, 783, 7
Colucci J. E., Bernstein R. A., Cohen J. G., 2014, ApJ, 797, 116
Colucci J. E., Bernstein R. A., McWilliam A., 2017, ApJ, 834, 105
Gallazzi A., Charlot S., Brinchmann J., White S. D. M., Tremonti C. A., 2005, MNRAS, 362, 41
García-Benito R., Pérez-Montero E., 2012, MNRAS, 423, 406
Geisler D., Smith V. V., Wallerstein G., Gonzalez G., Charbonnel C., 2005, AJ, 129, 1428
Hidalgo S. L., 2017, A&A, 606, A115
Kirby E. N., Lanfranchi G. A., Simon J. D., Cohen J. G., Guhathakurta P., 2011a, ApJ, 727, 78
Kirby E. N., Cohen J. G., Smith G. H., Majewski S. R., Sohn S. T., Guhathakurta P., 2011b, ApJ, 727, 79
Koch A., Grebel E. K., Gilmore G. F., Wyse R. F. G., Kleyna J. T., Harbeck D. R., Wilkinson M. I., Wyn Evans N., 2008, AJ, 135, 1580
Koleva M., de Rijcke S., Prugniel P., Zeilinger W. W., Michielsen D., 2009, MNRAS, 396, 2133
Kuntschner H. et al., 2006, MNRAS, 369, 497
Kuntschner H. et al., 2010, MNRAS, 408, 97
Larsen S. S., Brodie J. P., Strader J., 2017, A&A, 601, A96
Letarte B., 2007, PhD thesis, Univ. Groningen, the Netherlands
McDermid R. M. et al., 2015, MNRAS, 448, 3484
McWilliam A., Smecker-Hane T. A., 2005, ApJ, 622, L29
Majewski S. R., Hasselquist S., Łokas E. L., Nidever D. L., Frinchaboy P. M., García Pérez A. E., Johnston K. V., Mészáros S., 2013, ApJ, 777, L13
Makarova L., Koleva M., Makarov D., Prugniel P., 2010, MNRAS, 406, 1152
Mentz J. J., La Barbera F., Peletier R. F., Falcón-Barroso J., Lisker T., van de Ven G., Loubser S. I., Hilker M., 2016, MNRAS, 463, 2819
Michielsen D. et al., 2008, MNRAS, 385, 1374
Pipino A., Danziger I. J., 2011, A&A, 530, A22
Pompéia L. et al., 2008, A&A, 480, 379
Pritzl B. J., Venn K. A., Irwin M., 2005, AJ, 130, 2140
Roediger J. C., Courteau S., Graves G., Schiavon R. P., 2014, ApJS, 210, 10
Ruiz-Lara T. et al., 2015, A&A, 583, A60
Sakari C. M., Wallerstein G., 2016, MNRAS, 456, 831
Sbordone L., Bonifacio P., Buonanno R., Marconi G., Monaco L., Zaggia S., 2007, A&A, 465, 815
Schiavon R. P., 2007, ApJS, 171, 146
Schiavon R. P., Caldwell N., Conroy C., Graves G. J., Strader J., MacArthur L. A., Courteau S., Harding P., 2013, ApJ, 776, L7
Scott N. et al., 2013, MNRAS, 432, 1894
Şen Ş. et al., 2018, MNRAS, 475, 3453A
Shetrone M., Venn K. A., Tolstoy E., Primas F., Hill V., Kaufer A., 2003, AJ, 125, 684
Sybilska A. et al., 2017, MNRAS, 470, 815 (S17)

Thomas D., Maraston C., Bender R., Mendes de Oliveira C., 2005, ApJ, 621, 673
Toloba E., Guhathakurta P., Peletier R. F., Boselli A., Lisker T., Falcón-Barroso J., Simon J. D., van de Ven G., 2014, ApJS, 215, 17
Tolstoy E., Hill V., Tosi M., 2009, ARA&A, 47, 371
Tremonti C. A. et al., 2004, ApJ, 613, 898
van der Marel R. P., Kallivayalil N., 2014, ApJ, 781, 121
Vazdekis A., Sánchez-Blázquez P., Falcón-Barroso J., Cenarro A. J., Beasley M. A., Cardiel N., Gorgas J., Peletier R. F., 2010, MNRAS, 404, 1639
Vazdekis A. et al., 2015, MNRAS, 449, 1177
Watkins L. L., Evans N. W., An J. H., 2010, MNRAS, 406, 264
Wolf J., Martinez G. D., Bullock J. S., Kaplinghat M., Geha M., Muñoz R. R., Simon J. D., Avedo F. F., 2010, MNRAS, 406, 1220
Wyse R. F. G., 2010, in Cunha K., Spite M., Barbuy B., eds, Proc. IAU Symp. Vol. 265, Chemical Abundances in the Universe: Connecting First Stars to Planets. Cambridge Univ. Press, Cambridge, p. 461
Zolotov A., Willman B., Brooks A. M., Governato F., Hogg D. W., Shen S., Wadsley J., 2010, ApJ, 721, 738

APPENDIX A: [Mg/Fe] VERSUS [Fe/H] AS A FUNCTION OF GLOBAL σ

Here we provide the [Mg/Fe] versus [Fe/H] plots for the entire sample discussed in the paper (Fig. A1), analysed in bins of increasing $\sigma_{\rm local}$ (shown in the main text), $\sigma_{\rm global}$, as well as the second velocity moment $V_{\rm rms}$, with the view to providing reference for future studies and comparisons involving a variety of object and data types. We note that the plots involving the three quantities are in excellent agreement.

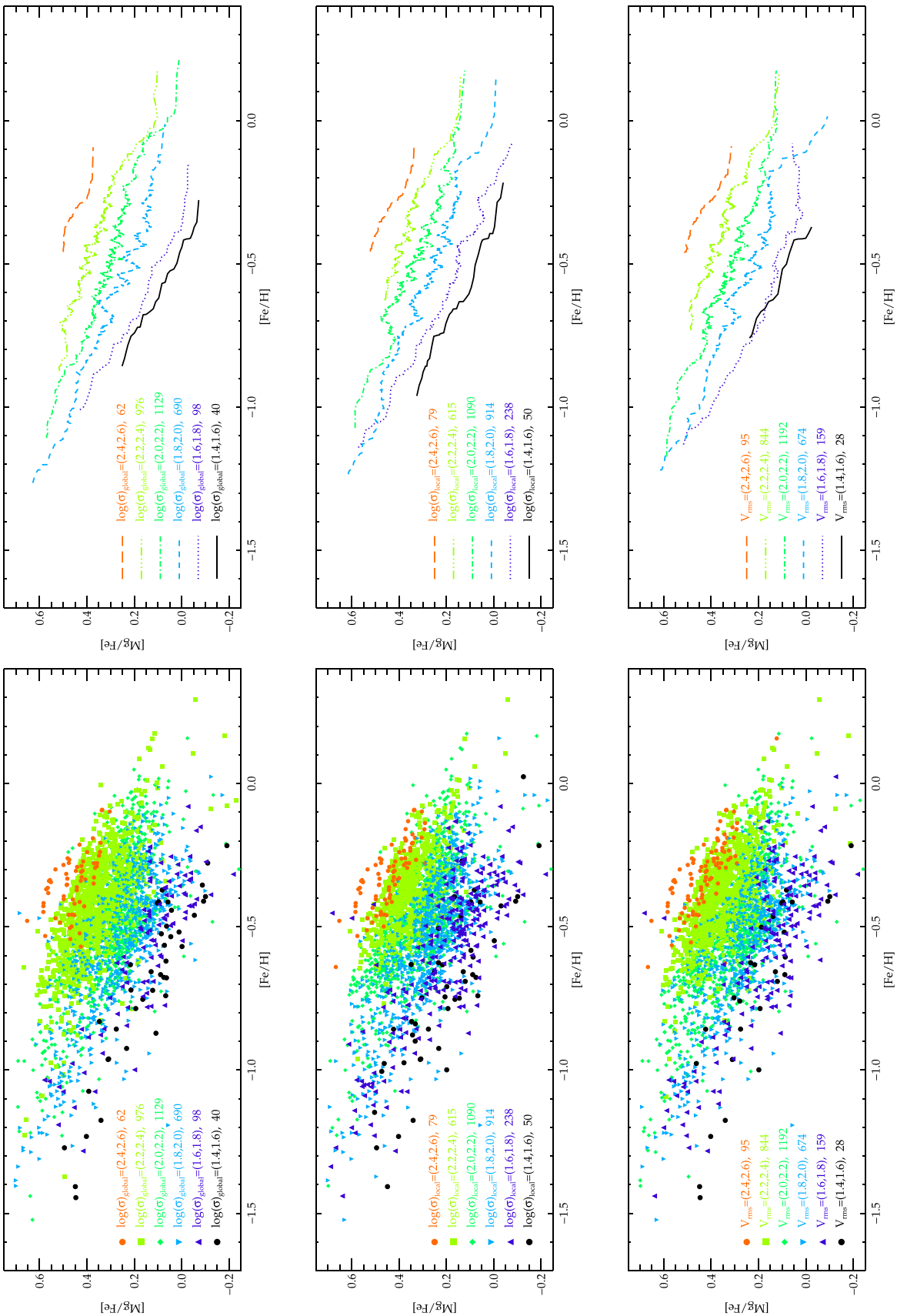

Figure A1. As in Fig. 2 but for comparison colour coded by $\sigma_{\rm global}$ (left), $\sigma_{\rm local}$ (middle), and $V_{\rm rms}$ values. For each of the quantities all individual profile points and running averages are shown.

This paper has been typeset from a TEX/LATEX file prepared by the author.